12th International Symposium on Turbulence and Shear Flow Phenomena (TSFP12)
Osaka, Japan (Online), July 19-22, 2022

VELOCITY SPECTRA AND SCALE DECOMPOSITION OF ADVERSE PRESSURE GRADIENT TURBULENT BOUNDARY LAYERS

Sylvia K. Romero
Department of Mechanical Engineering
University of Melbourne
700 Swanston St., Parkville, Victoria 3010 Australia
sylviar@student.unimelb.edu.au

Spencer J. Zimmerman
Department of Mechanical Engineering
Johns Hopkins University
3910 Keswick Road, Baltimore, MD 21218 USA
zimmerman@jhu.edu

Jimmy Philip
Department of Mechanical Engineering
University of Melbourne
700 Swanston St., Parkville, Victoria 3010 Australia
jimmyp@unimelb.edu.au

Joseph C. Klewicki
Department of Mechanical Engineering
University of Melbourne
700 Swanston St., Parkville, Victoria 3010 Australia
klewicki@unimelb.edu.au

ABSTRACT

Adverse pressure gradient turbulent boundary layer velocity spectra at high Reynolds number ($7100 \leq Re_\tau \leq 8600$) are compared to a zero pressure gradient case from Zimmerman (2019); Zimmerman *et al.* (2019) at matching Reynolds number. Wall-distance scaling observed in the zero pressure gradient spectra is also observed in the adverse pressure gradient spectra. Effects of varying Re_τ on the velocity variances and Reynolds shear stress are studied by comparing the present data with the data of Monty *et al.* (2011) at lower Re_τ (≈ 1900) and varying Clauser pressure gradient parameter β. Cases at similar β and Reynolds number, but with varying flow history are also studied. Increases are observed in the outer peak of $\overline{u^2}^+$, $\overline{v^2}^+$, and $-\overline{uv}^+$. Under a scaling that uses a hybrid velocity u_{hyb} there is similarity between the outer region profiles of spectrally-decomposed variances and Reynolds shear stress.

INTRODUCTION

The behavior of the streamwise variance $\overline{u^2}$, wall-normal variance $\overline{v^2}$, and Reynolds shear stress $-\overline{uv}$ as well as their premultiplied (co)spectra k_xE are analyzed to see how the energy distributions are affected by an increasing pressure gradient. Here, $k_x = 2\pi f/U$ is the streamwise wavenumber, where f is the frequency and U is the mean streamwise velocity at a particular wall-normal location y. E is the spectral density of the velocity fluctuations. The integration of E at a wall-normal location across all wave numbers results in the (co)variance at that wall-location. To study the relationship between the premultiplied (co)spectra, wavelength, and wall-distance, in the present study the premultiplied (co)spectra are plotted as contour-maps that are a function of wavelength and wall-distance.

In the present study two velocity scales are studied: the friction velocity scale u_τ and a velocity scale u_{hyb} introduced in Romero *et al*. (2022*a*). This velocity scale, $u^2_{hyb} \equiv u^2_\tau + \frac{y}{\rho}\frac{dP}{dx}$ (with ρ the fluid density) exhibited reasonable success in scaling the Reynolds stress over a range of β and Reynolds number relative to the y-independent velocity scales studied. A degree of the success of this velocity scale is in some sense guaranteed by its construction, which is based on the dominant terms in the mean stress balance most responsible for balancing the turbulent momentum flux.

The premultiplied (co)spectra normalized by viscous scales ($k_x u_\tau^{-2} E$) are compared to the premultiplied (co)spectra normalized by u_{hyb} (i.e., $k_x u_{hyb}^{-2} E$). The premultiplied (co)spectra are presented in terms of streamwise wavelength λ_x normalized by viscous scales ν/u_τ (to obtain λ_x^+) and outer scales δ (to obtain λ_x/δ), where ν is the kinematic viscosity and the boundary layer thickness is δ. The effects of u_τ normalization and u_{hyb} normalization on the magnitude of the premultiplied streamwise, wall-normal, and (co)spectra of an adverse pressure gradient turbulent boundary layer (APG TBL) are compared to a zero pressure gradient (ZPG) case from Zimmerman (2019); Zimmerman *et al.* (2019) at matching $Re_\tau = \delta u_\tau/\nu$. The spectra are not shown in Zimmerman *et al.* (2019), but the dataset is qualified and described.

The two-dimensional x-momentum Reynolds-averaged Navier-Stokes (RANS) equation for a statistically stationary APG TBL is

$$\frac{\partial^2 U^+}{\partial y^{2+}} + \frac{\partial(-\overline{uv}^+)}{\partial y^+} + \left[-U^+\frac{\partial U^+}{\partial x^+} - V^+\frac{\partial U^+}{\partial y^+}\right] + U^+_\infty \frac{\partial U^+_\infty}{\partial x^+} = 0. \tag{1}$$

This is also called the mean momentum equation. Here a superscript plus denotes normalization by ν, and u_τ. Note that $\partial(-\overline{uv}^+)/\partial y^+$, also known as the turbulent inertia (TI) term in the RANS equation in (1), is related to the differentiated cospectra of $-\overline{uv}$ as follows:

$$\frac{\partial(-\overline{uv})}{\partial y} = \int_0^\infty \left(\frac{\partial E_{uv}}{\partial y}\right) dk_x. \tag{2}$$

The differentiated cospectra are also analyzed in this paper as this facilitates consideration of the length scales associated with net momentum increase (sources) versus loss (sinks) and their variations with distance from the wall. Furthermore, the zero-crossing of the TI term corresponds to the peak location of the Reynolds shear stress. This location is of particular importance since the zero-crossing of the TI term marks the mean transition from momentum source to momentum sink for the flow as a whole.

In the present study we will also show the effects of u_τ normalization and u_{hyb} normalization on the spectrally decomposed streamwise variance, wall-normal variance, and Reynolds shear stress profiles of an APG TBL as compared to a ZPG case. The behavior of $\overline{u^2}$ is also compared using cases from Monty *et al.* (2011). From observing the viscous-scaled mean statistics, it has been previously noted by Bobke *et al.* (2017) and Sanmiguel Vila *et al.* (2017) that flows with increasing β exhibit behavior of an upstream smaller β, while flows with decreasing β exhibit behaviors of an upstream larger β. To further analyze this behavior, cases at similar β and Reynolds numbers, but with varying flow history are also compared.

EXPERIMENTS

Facility and ramp

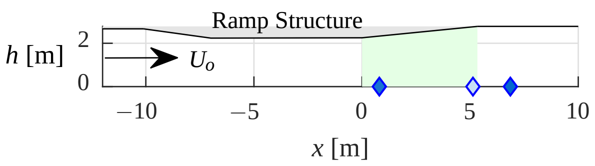

Figure 1. Current flow geometry and measurement locations. Area shaded in green is along APG ramp. Arrow points in flow direction. Measurement locations given in table 1.

The present measurements were collected in the Flow Physics Facility (FPF) at the University of New Hampshire. The FPF test section features a 2.8m × 6m inlet cross-section and a downstream development fetch of 72m. Streamwise pressure gradients for the present measurements were generated via ceiling panels installed ≈31m downstream of the wind tunnel inlet, cf. figure 1. This ≈15m long ceiling insert consisted of an initial 3.1m favorable pressure gradient (FPG) region, followed by a 7.0m ZPG region (where the flow relaxes back to a nearly canonical state), and finally a 5.3m APG region. The flow was then allowed to develop downstream under ZPG conditions for the remaining 20m of tunnel fetch. Pressure distribution measurements support that the ZPG ramp is sufficiently long since the streamwise pressure gradient dP/dx versus x equilibrates along the ZPG section. The relatively long ZPG ramp ensures approximately ZPG flow (or at worst a very mild FPG) before the APG ramp. Measurements along the APG ramp where β is increasing are compared to measurements taken downstream of the ramp insert where β is decreasing. The data in the present paper is a subset of a larger data set. Part of this data set has been previously published in Romero *et al.* (2021, 2022*b*). The present data locations are given in figure 1.

Measurement Probe and Parameters

Hot-wire measurements were obtained along the APG section and downstream of the ramp insert using a three-wire hot-wire probe based on the design of Kawall *et al.* (1983). This probe consists of a single wire orthogonal to the mean flow direction and two wires arranged as an ×-array, with the single wire located between two ×-array wires. The non-dimensional wire length of the single wire is $l^+ = lu_\tau/\nu = 17.6$, while the length of the ×-array wires projected onto the $y-z$ plane is $l^+/\sqrt{2}$.

The effects of pressure gradients on TBLs are often parameterized in terms of the Clauser pressure-gradient parameter $\beta = (\delta^*/\tau_w)(dP/dx)$, where δ^* is the displacement thickness and τ_w is the wall shear stress. Positive and negative values of β respectively reflect APG and FPG conditions, while $\beta = 0$ reflects ZPG conditions. Self-preserving APG TBLs are characterized by nominally constant β and Re_τ, (e.g., Townsend, 1956; Tennekes & Lumley, 1972). In the present study β increases mildly to about 2 while Re_τ grows slowly. A summary of the experiments is given in table 1. $U_\infty = U(y = \delta)/0.99$ is the freestream velocity, and $\Delta t_s^+ = (1/f_s)u_\tau^2/\nu$ is the non-dimensionalised sample interval, where f_s is the sampling frequency.

Table 1. Summary of present experiments. The distance x [m] is the distance downstream from the start of the APG ramp section. The APG ramp ends at x=5.3m. Arrows indicate whether β is increasing or decreasing with distance x. Z19 refers to Zimmerman (2019) and M11 to Monty *et al.* (2011).

Source	x [m]	β	U_∞ [m/s]	u_τ [m/s]	δ[m]	Re_τ	Δt_s^+
present	0.80	0.9 ↑	7.91	0.26	0.42	7100	0.30
	5.13	1.8 ↑	7.11	0.22	0.57	7770	0.20
	6.86	0.8 ↓	7.05	0.23	0.59	8600	0.22
Z19	-	0	6.47	0.23	0.50	7880	0.24
M11	-	0	-	-	-	1820	-
	-	0.8 ↑	-	-	-	1860	-
	-	1.8 ↑	-	-	-	1940	-

SPECTRA AND SCALE DECOMPOSITION

Constant Re_τ

The ZPG TBL and APG TBL $k_x u_\tau^{-2} E$ and $k_x u_{hyb}^{-2} E$ are compared in figures 2 and 3, respectively. The ZPG cases are plotted in figures 2(a-d) and 3(a-c). The APG TBL plots under u_τ scaling are presented in figure 2(e-p), while the plots under u_{hyb} scaling are shown in figure 3(d-1).

Spectra under u_τ scaling: In comparison to the ZPG case the outer region of the APG case gets energized relative to the inner region when normalized by u_τ. This behavior is observed in the viscous-scaled premultiplied streamwise spectra ($k_x^+ E_{uu}^+$), wall-normal spectra ($k_x^+ E_{vv}^+$), and cospectra ($k_x^+ E_{uv}^+$). Similar behavior are reflected in the $\overline{u^2}^+$, $\overline{v^2}^+$, and $-\overline{uv}^+$ profiles, plotted in solid green lines, in figure 4(b), figure 5(a), and figure 5(c), respectively, where a distinct outer peak forms with increasing β. This reflects the decoupling of the rate of momentum flux from the wall shear stress (that otherwise characterizes ZPG BLs) with the addition of the non-zero pressure gradient term.

For the ZPG TBL $k_x^+ E_{uu}^+$ the inner peak is fixed in viscous units at $y^+ \simeq 15$ and $\lambda_x^+ \simeq 1000$, (e.g., Hutchins & Marusic, 2007; Harun, 2012). Although the inner peak is not completely captured in the APG TBL $k_x^+ E_{uu}^+$, it appears that the inner peak remains at $\lambda_x^+ \simeq 1000$; see figures 2(e, i, m). For the ZPG TBL

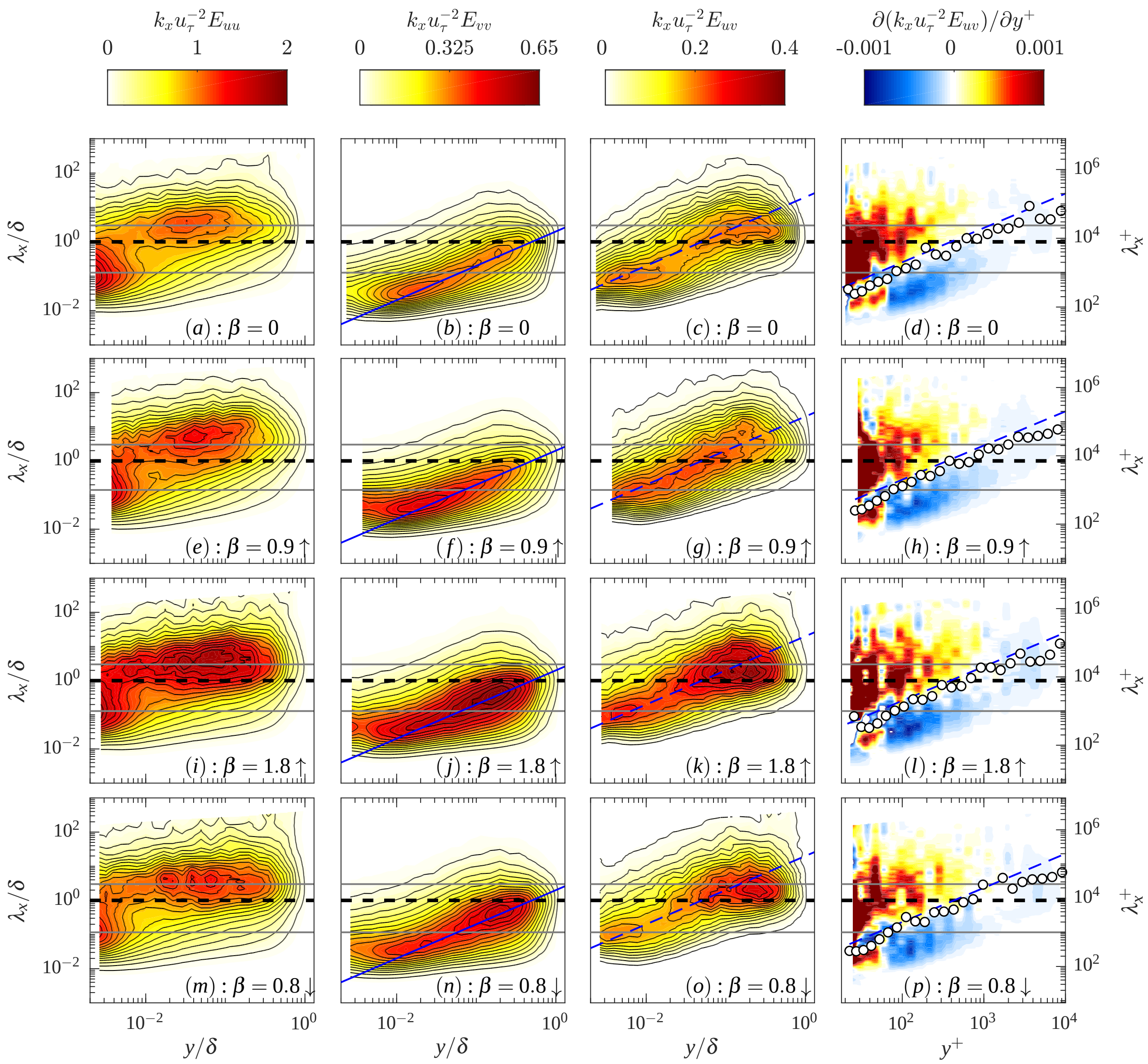

Figure 2. Premultiplied energy spectra normalized by u_τ. Starting from left, first column: streamwise spectra, second column: wall-normal spectra, third column: cospectra of $-\overline{uv}$, and fourth column: derivative of cospectra. (a-d) $\beta = 0$ at $Re_\tau = 7880$ from Zimmerman (2019), (e-h) $\beta = 0.9$ at $Re_\tau = 7100$, (i-l) $\beta = 1.8$ at $Re_\tau = 7800$, and (m-p) $\beta = 0.8$ at $Re_\tau = 8600$. Thick black dashed line at $\lambda_x/\delta = 1$. Grey solid lines at $\lambda_x^+ = 1000$ and $\lambda_x/\delta = 3$. Blue solid line at $\lambda_x = 2y$. Blue dashed line at $\lambda_x = 20y$. The circles denote $20W(y^+)$. Cases given in table 1.

the inner peak of $k_x^+ E_{uv}^+$ also appears near $\lambda_x^+ \simeq 1000$. This trend continues in the APG TBL $k_x^+ E_{uv}^+$ in figures 2(g, k, o).

In the outer region the $k_x^+ E_{uu}^+$ for both the ZPG and APG cases, the most energetic motions occur near $\lambda_x/\delta \approx 3$, as seen in figures 2(a, e, i, m). For the ZPG case, the outer peak of $k_x^+ E_{uv}^+$ also seems to appear near $\lambda_x/\delta \approx 3$, but perhaps at a slightly smaller λ_x/δ, as seen in figure 2(c). This behavior is also seen in the APG TBL; see figures 2(g, k, o).

The most energetic motions reflected in the wall-normal spectra $k_x^+ E_{vv}^+$ follow the $\lambda_x = 2y$ trend line for both the ZPG and APG cases. This wall-distance scaling is also exhibited in the cospectra for $y/\delta \lessapprox 0.15$, where the areas of high magnitude follow the $\lambda_x = 20y$ trend line. Despite the differences in energy density relative to the local wall-shear-stress scale, the presence of the pressure gradient has evidently little effect on the relative scales of modes that are set by wall-distance or the boundary layer thickness.

The derivative of the cospectra are plotted in figures 2(d, h, l, p). The local peak in $k_x^+ E_{uv}^+$ corresponds to the zero-crossing of $\partial(k_x^+ E_{uv}^+)/\partial y^+$, which also roughly follows the $\lambda_x = 20y$ trend line. This emphasizes the robustness of wall-distance scaling in the transition from momentum source to momentum sink like motions as the wavelength changes. It appears that eddy structures that are approximately smaller than $\lambda_x = 20y$ contribute to a negative momentum flux (or sinks) whereas larger λ_x leads to a momentum source. Here the analogy with viscous stress gradient, which is always a sink, is particularly useful. At smaller scales turbulence could be assumed to behave in an almost random manner, which is analogous to the random molecular motion (leading to viscosity), resulting in a sink of momentum. On the hand, larger scales are only capable of bringing momentum to the wall (likely from the outer region) rather than taking momentum away from the wall (because the wall will restrict the existence of large structures that can carry momentum away from the wall) making them an overall momentum source.

For the ZPG TBL, a length scale distribution W^+ that allows the mean momentum equation to be written in a self-similar form is defined (e.g., in Morrill-Winter *et al.*, 2017*a*) as:

$$W^+(y^+) = \left(\frac{\partial^2 U^+}{\partial {y^+}^2}\right)^{-1/2}. \quad (3)$$

The distribution of $20W^+(y^+)$ markers are plotted in figures 2(d, h, l, p) as circles. Due to the difficulty of taking the second derivative of the experimental mean velocity profiles, these profiles are not definitive, but do appear to exhibit wall-distance scaling. In Morrill-Winter *et al.* (2017*b*) it is noted for a ZPG TBL that the distribution of $20W^+(y^+)$ roughly coincides with the zero-crossing of the differentiated cospectra. This is also observed in the present APG TBL plots.

Spectra under u_{hyb} scaling: Figure 3 shows spectra in u_{hyb} scaling, where we observe that for $y/\delta \gtrsim 0.1$ the $k_x u_{hyb}^{-2} E_{uu}$, $k_x u_{hyb}^{-2} E_{vv}$, and $k_x u_{hyb}^{-2} E_{uv}$ magnitudes decrease relative to the ZPG case. Similarity is evidenced between the APG cases in this region. This is also observed for the $\overline{u^2}^*$ in figure 4(d), $\overline{v^2}^*$ in figure 5(b), and $-\overline{uv}^*$ for figure 5(d). The profiles of the APG cases fall below the ZPG case in the outer region. Here superscript $*$ represents u_{hyb} scaling.

Stronger β trends are observed for $y/\delta \lesssim 0.1$. In this region $k_x u_{hyb}^{-2} E_{uu}$, $k_x u_{hyb}^{-2} E_{vv}$, and $k_x u_{hyb}^{-2} E_{uv}$ increase with increasing β. Like the $k_x^+ E_{uu}^+$, the energetic outer region of $k_x u_{hyb}^{-2} E_{uu}$ occurs in the vicinity of $\lambda_x/\delta \approx 3$, but has moved inwards towards the wall. Near the wall ($y/\delta \lesssim 10^{-2}$), the spectra under u_{hyb} scaling behave similar to the spectra under u_τ scaling since u_{hyb} approaches u_τ at the wall by construction.

For $y/\delta \gtrsim 10^{-2}$ the areas of high magnitude in $k_x u_{hyb}^{-2} E_{vv}$ exhibit wall-scaling near the $\lambda_x = 2y$ line; see figures 3(e, h, k). Again, wall-distance scaling is also observed in the cospectra, but along $\lambda_x = 20y$; see figures 3(f, i, l).

Changes with flow history: The effectiveness of u_{hyb} for APG cases at similar β and Reynolds number, but with varying flow history, are now compared. In this section a case where β is just increasing from 0 (the $\beta = 0.9 \uparrow$ case), is compared to a case where β is decreasing and the flow has had longer time to develop (the $\beta = 0.8 \downarrow$ case).

Now looking at $k_x u_{hyb}^{-2} E_{uu}$, in figure 3(d) β is just increasing from 0, while in figure 3(j) β is decreasing and the flow has had longer time to develop. The APG case in figure 3(j) where β is decreasing has a slightly higher outer region than the case where β is increasing in figure 3(d). This is similarly observed in the outer region of the $\overline{u^2}^*$ profiles in figure 4(d). In the inner region ($y/\delta \lesssim 10^{-2}$) of the $\overline{u^2}^*$ profile the decreasing β profile shows stronger similarity to the ZPG case than the increasing β profile, see figure 4(d). This suggests that agreement between ZPG profiles and APG profiles subjected to u_{hyb} scaling may improve as the development length/time of the APG case increases.

To quantify the contribution of the small-scale and large-scale motions, the streamwise variance is decomposed into small-scale and large-scale components by using a sharp spectral cut-off. The choice of the appropriate cut-off wave-length λ_{x-cut} in the present analysis follows the work of Mathis *et al.* (2009), where $\lambda_{x-cut} = \delta$ is used since it appears to separate the large and small-scale velocity components of $k_x^+ E_{uu}^+$ of a ZPG TBL at $Re_\tau = 7300$. This also seems to be an appropriate cut-off wave-length of the present data, where a thick dashed line plotted at $\lambda_x/\delta = 1$ separates the inner and outer energy peaks, as seen in figures 2(a, e, i, m). For completeness, the wall-normal variance and Reynolds shear stress are also decomposed using the same cut-off wave-length $\lambda_{x-cut} = \delta$ to see where attributes of the streamwise measurements appear in the wall-normal variance and Reynolds shear stress profiles.

The behavior of the decomposed streamwise variance profiles $\overline{u^2}^+$ versus $\overline{u^2}^*$ are compared in figure 4. The decomposed wall-normal variance profiles $\overline{v^2}^+$ versus $\overline{v^2}^*$ and decomposed Reynolds shear stress $-\overline{uv}^+$ versus $-\overline{uv}^*$ are compared in figure 5. The original APG TBL profiles are plotted in solid green lines, while the small-scale components are plotted as blue dashed-dot lines and the large-scale components are plotted as orange dashed lines. The respective ZPG profiles are plotted in black.

In the outer region of the large-scale components of $\overline{u^2}^*$, $\overline{v^2}^*$, and $-\overline{uv}^*$ there is stronger similarity between the APG cases where β is increasing ($\beta = 0.9$ and 1.8) than to the case where β is decreasing ($\beta = 0.8$), see figure 4(d), figure 5(b), and figure 5(d), respectively. Whether scaled by u_τ or u_{hyb}, in the inner region of the large-scale components, the cases at similar β(= 0.8 and 0.9) behave more like one another than the $\beta = 1.8$ case.

Now looking at the small-scale components, there is very strong similarity between the two increasing β cases ($\beta = 0.9$ and 1.8) throughout the $\overline{u^2}^*$ profile and in the $-\overline{uv}^*$ profile for $y/\delta \gtrsim 10^{-2}$. There is slightly more scatter in the $\overline{v^2}^*$ profiles.

Overall under u_{hyb} scaling, the decreasing β measurements have a slight increase towards the ZPG case in the outer region of the profiles, but still behave similarly to the ramp measurements.

Changes with Re_τ

The present measurements at $7100 \leq Re_\tau \leq 8600$ (in figures 4(b, d)) are compared to profiles at matching β from Monty *et al.* (2011) at $Re_\tau \approx 1900$ (in figures 4(a, c)).

The results of figures 4(a, c) indicate that at low Reynolds number there is relatively little change with β in the small-scale components near the inner peak for both u_τ and u_{hyb} scaling. While the inner peak is not completely captured in figures 4(b, d), there is a larger increase in the small-scale components in the near-wall region from the ZPG to the APG cases. The outer flow appears to have a stronger influence on the inner flow at these large Reynolds numbers.

Both the small-scale and large-scale components under u_τ scaling have increased from the ZPG case to APG case but, larger increases are seen in the large-scale components in the outer region. In the ZPG case, the large-scale components exhibit an outer peak that is denoted by a vertical line at $y/\delta \approx 0.1$ in figures 4(a-d). Under u_τ scaling the outer region increases with increasing β (see figures 4(a-b)), while under u_{hyb} scaling there is strong similarity between the APG cases in the outer region (see figures 4(c-d)).

CONCLUSIONS

Increases are seen in the magnitude of $k_x^+ E_{uu}^+$, $k_x^+ E_{vv}^+$, $k_x^+ E_{uv}^+$ and in the outer peak of $\overline{u^2}^+$, $\overline{v^2}^+$, and $-\overline{uv}^+$ as β increases. Under u_{hyb} scaling, the APG TBL premultiplied

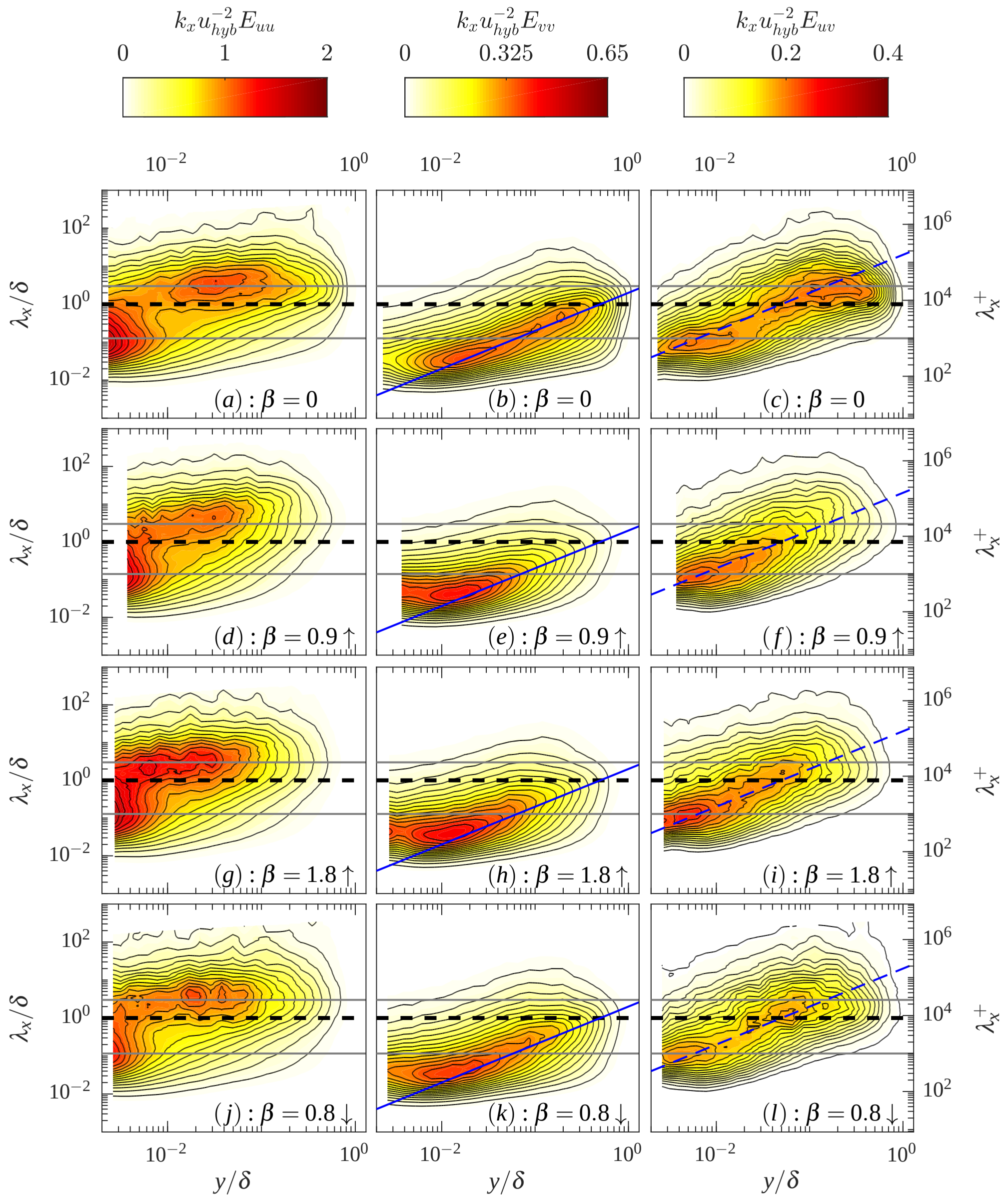

Figure 3. Premultiplied energy spectra normalized by u_{hyb}. Starting from left, first column: streamwise spectra, second column: wall-normal spectra, and third column: cospectra of $-\overline{uv}$. (a-c) $\beta = 0$ at $Re_\tau = 7880$ from Zimmerman (2019), (d-f) $\beta = 0.9$ at $Re_\tau = 7100$, (g-i) $\beta = 1.8$ at $Re_\tau = 7800$, and (j-l) $\beta = 0.8$ at $Re_\tau = 8600$. Thick black dashed line at $\lambda_x/\delta = 1$. Grey solid lines at $\lambda_x^+ = 1000$ and $\lambda_x/\delta = 3$. Blue solid line at $\lambda_x = 2y$. Blue dashed line at $\lambda_x = 20y$. Cases given in table 1.

(co)spectra and (co)variances behave similarly to one another, but decrease relative to the ZPG case in the outer region. The small-scale and large-scale components of the decomposed $\overline{u^2}^*$, $\overline{v^2}^*$, and $-\overline{uv}^*$ APG profiles also exhibit similarity in the outer region over a range of Re_τ. Based on the similarity between APG cases, these findings indicate that u_τ scaling performs well in the inner region, while u_{hyb} scaling is more appropriate in the outer region regardless of scale.

Wall-distance scaling observed in the wall-normal spectra appears to contribute to the wall-distance scaling seen in the cospectra. Observations of the differentiated cospectra highlight that the transition from momentum source to sink scales with wall-distance for both increasing and decreasing β cases. The robustness of wall-distance scaling is further emphasized by the behavior of W^+ profiles for the APG cases studied.

REFERENCES

Bobke, A., Vinuesa, R., Örlü, R. & Schlatter, P. 2017 History effects and near equilibrium in adverse-pressure-gradient turbulent boundary layers. *J. Fluid Mech.* **820**, 667–692.

Harun, Z. 2012 The structure of adverse and favourable pressure gradient turbulent boundary layers. PhD thesis.

Hutchins, N. & Marusic, I. 2007 Large-scale influences in near-wall turbulence. *Philosophical Transactions of the Royal Society A: Mathematical, Physical and Engineering Sciences* **365** (1852), 647–664.

Kawall, J. G., Shokr, M. & Keffer, J. F. 1983 A digital technique for the simultaneous measurement of streamwise and lateral velocities in turbulent flows. *J. Fluid Mech.* **133**, 83–112.

Mathis, R., Hutchins, N. & Marusic, I. 2009 Large-scale amplitude modulation of the small-scale structures in turbulent boundary layers. *J. Fluid Mech.* **628**, 311–337.

Monty, J.P., Harun, Z. & Marusic, I. 2011 A parametric study

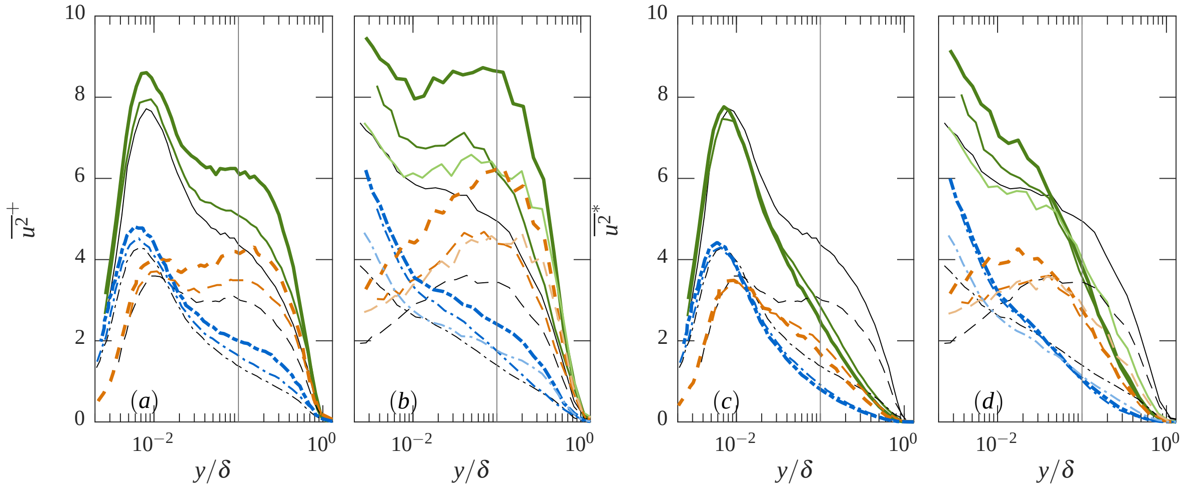

Figure 4. Decomposition of the broadband streamwise variance profile (a-b) scaled by u_τ^2 and (c-d) scaled by u_{hyb}^2. (a, c) $\beta = 0, 0.8$, and 1.8 at $Re_\tau \approx 1900$ and $(15 \leq l^+ \leq 17)$ from Monty *et al.* (2011). (b, d) $\beta = 0$, 0.9, 1.8, and 0.8 at $7100 \leq Re_\tau \leq 8600$ and $(16 \leq l^+ \leq 20)$. APG profiles plotted in color, respective ZPG profiles plotted in black. Total profile for APG cases plotted as solid green lines. Small-scale component $(\lambda_x < \delta)$ plotted as blue dashed-dot lines and large-scale component $(\lambda_x > \delta)$ plotted as orange dashed lines. Line thickness increases with increasing β. The present $\beta = 0.8 \downarrow$ case is plotted in lighter shades to differentiate from the $\beta = 0.9 \uparrow$ case. Vertical line plotted at $y/\delta = 0.1$.

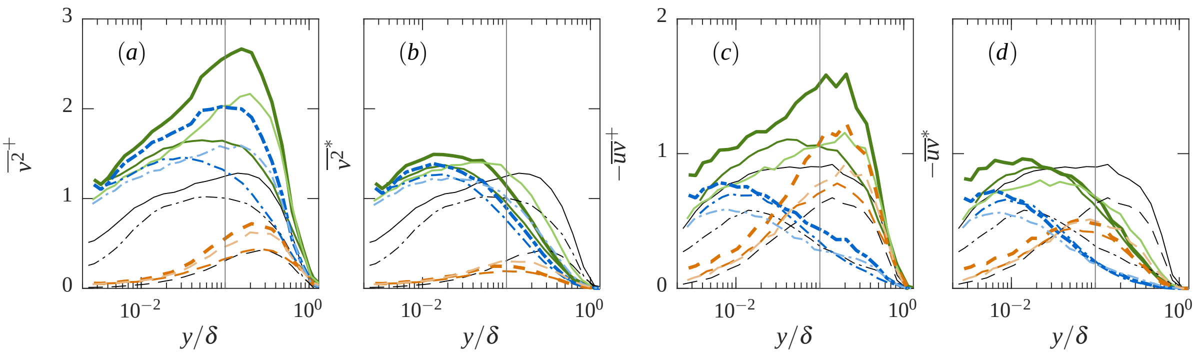

Figure 5. Decomposition of the broadband (a-b) wall-normal variance and (c-d) Reynolds shear stress profiles. (a, c) scaled by u_τ^2 (b, d) scaled by u_{hyb}^2. APG profiles plotted in color, respective ZPG profiles plotted in black. Total profile for APG cases plotted as solid green lines. Small-scale component $(\lambda_x < \delta)$ plotted as blue dashed-dot lines and large-scale component $(\lambda_x > \delta)$ plotted as orange dashed lines. Line thickness increases with increasing β. $\beta = 0$, 0.9, 1.8, and 0.8 at $7100 \leq Re_\tau \leq 8600$ and $(16 \leq l^+ \leq 20)$. The present $\beta = 0.8 \downarrow$ case is plotted in lighter shades to differentiate from the $\beta = 0.9 \uparrow$ case. Vertical line plotted at $y/\delta = 0.1$.

of adverse pressure gradient turbulent boundary layers. *Int. J. Heat Fluid Flow* **32** (3), 575–585.

Morrill-Winter, C., Philip, J. & Klewicki, J. 2017*a* An invariant representation of mean inertia: theoretical basis for a log law in turbulent boundary layers. *J. Fluid Mech.* **813**, 594–617.

Morrill-Winter, C., Philip, J. & Klewicki, J. 2017*b* Statistical evidence of anasymptotic geometric structure to the momentum transporting motions in turbulent boundary layers. *Philosophical Transactions of the Royal Society A: Mathematical, Physical and Engineering Sciences* **375** (2089), 20160084.

Romero, S., Zimmerman, S., Philip, J. & Klewicki, J. 2021 Characteristics of reynolds shear stress in adverse pressure gradient turbulent boundary layers. In *iTi Conference on Turbulence*, pp. 173–179. Springer.

Romero, S., Zimmerman, S., Philip, J. & Klewicki, J 2022*a* Stress equation based scaling framework for adverse pressure gradient turbulent boundary layers. *Int. J. Heat and Fluid Flow* **93**, 108885.

Romero, S., Zimmerman, S., Philip, J., White, C. & Klewicki, J. 2022*b* Properties of the inertial sublayer in adverse pressure-gradient turbulent boundary layers. *J. of Fluid Mech.* **937**.

Sanmiguel Vila, C., Örlü, R., Vinuesa, R., Schlatter, P., Ianiro, A. & Discetti, S. 2017 Adverse-pressure-gradient effects on turbulent boundary layers: statistics and flow-field organization. *Flow Turbul. Combust.* **99** (3-4), 589–612.

Tennekes, H. & Lumley, J. L. 1972 *A First Course in Turbulence*. The MIT Press.

Townsend, A.A. 1956 The structure of turbulent shear flow. *Cambridge University* **15**.

Zimmerman, S. 2019 Experimental investigation of velocity and vorticity in turbulent wall flows. PhD thesis, The University of Melbourne.

Zimmerman, S., Philip, J., Monty, J., Talamelli, A, Marusic, I., Ganapathisubramani, B., Hearst, R.J., Bellani, G., Baidya, R., Samie, M. *et al.* 2019 A comparative study of the velocity and vorticity structure in pipes and boundary layers at friction Reynolds numbers up to 10^4. *J. Fluid Mech* **869**, 182–213.